Materials & Design 223 (2022) 111173

Contents lists available at ScienceDirect

Materials & Design

journal homepage: www.elsevier.com/locate/matdes

Biomechanical behavior of customized scaffolds: A three-dimensional finite element analysis

Jessica León de Ulloa [a], Jesús E. González [a], Ana M. Beltrán [b,*], Eduardo Peón Avés [a], Jennifer Rodríguez-Guerra [a], Yadir Torres [b]

[a] Departamento de Biomateriales Cerámicos y Metálicos, Centro de Biomateriales, Universidad de La Habana, La Habana 6323, Cuba
[b] Departamento de Ingeniería y Ciencia de los Materiales y el Transporte, Escuela Politécnica Superior, Universidad de Sevilla, 41011 Sevilla, Spain

HIGHLIGHTS

- Design and simulation by FEM of customized scaffolds fixed to the jaw by a dental implant.
- Distribution of stress in crown, dental implant, scaffold, cortical and trabecular bone, and strain in the cortical and trabecular bone.
- Influence of the porosity and hole size of the scaffolds on the stress and strain in the cortical and trabecular bone.
- The use of customized scaffolds allows a significant reduction in stresses and strain in the peri-implant cortical bone.

GRAPHICAL ABSTRACT

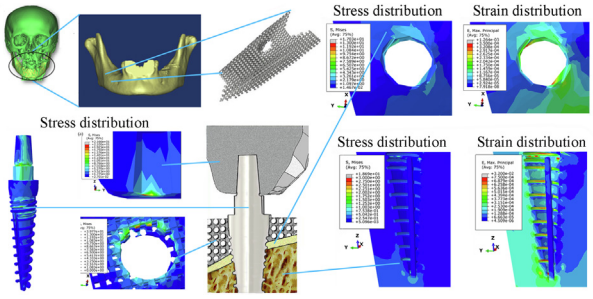

ARTICLE INFO

Article history:
Received 7 July 2022
Revised 15 September 2022
Accepted 17 September 2022
Available online 19 September 2022

Keywords:
Finite element analysis
Customized scaffold
Biomechanical behavior
Edentulous jaw
Dental implants

ABSTRACT

Teeth loss due to periodontal diseases, trauma, or infections often causes dimensional loss in the affected maxillary. In patients with reduced maxillary size, restoration of chewing function and esthetics with endosseous dental implants may fail. The aim of this work was to simulate the biomechanical behavior, using the finite element method, of customized scaffolds fixed by a dental implant on a partially edentulous jaw. Porous scaffolds were designed from medical images of a partially edentulous jaw with type IV bone quality. The influence of the diameter of the hole and the porosity of the scaffold on the maximum levels of stress and strain in the *peri*-implant bone was evaluated. The highest stress values in the scaffolds, dental implant, and crown were lower than the yield strength of their respective materials. The customized scaffolds allow to recover the dimensions of the evaluated jaw. A significant decrease in stress and strain values was observed in the *peri*-implant cortical bone. Furthermore, it was found that the evaluated parameters did not have a significant influence on the maximum von Mises equivalent stress and maximum strain values in the *peri*-implant bone.

1. Introduction

Teeth loss due to periodontal diseases, trauma, or infection of the alveolar bone often leads to surgical intervention to restore the jaws [1]. Recent advances in biomaterials have contributed to the increase in available options for bone regeneration in atrophied

* Corresponding author.
E-mail address: abeltran3@us.es (A.M. Beltrán).

https://doi.org/10.1016/j.matdes.2022.111173
0264-1275/

jaws of partially or completely edentulous patients (use of bone grafts, placement of sub-periosteal dental implants, use of stem cells, among others) [2,3]. However, these options presented multiple limitations [2,4]. In addition, in atrophied jaws, the clinical success rate of endosseous dental implants can be significantly reduced [5].

For these reasons, several works report the development of porous scaffolds that allow bone regeneration in the affected area of the jaws [3,6,7]. A wide range of materials (including polymers, ceramics, metals and composites) are used in the manufacture of scaffolds for bone regeneration [8–10], which provide a suitable environment for tissue regeneration. Titanium and its alloys, specifically Ti6Al4V, are among the most widely used metallic materials, due to their biocompatibility and mechanical properties [11–13]. Furthermore, the use of porous structures is an effective option to reduce the mismatch of the elastic modulus presented by some biomaterials with bone [9,14–16]. Therefore, porous titanium scaffolds reduce stress shielding, fit well with host bone, reduce bone absorption, stimulate rapid bone formation and integration at the bone-implant interface [16,17], show a higher fixation ability than bulk implants, and achieve sufficient biological stability in a short time [18]. In bioactive material scaffolds, bone tissue grows inside pores and, in addition, pores with rough walls improve osseointegration. A scaffold with a pore diameter of at least 300 μm facilitates the transport of nutrients and, ultimately, osteogenesis. Unfortunately, scaffolds with pores smaller than 100 μm, although showing high mechanical properties, tend to cause hypoxic conditions in the microenvironment that favor osteochondral formation and not osteogenesis. With pores larger than 800 μm, there is ample space for the vascularization and delivery of precursor cells from the osteoclast and osteoblast lineages, but their mechanical strength is low [19,20]. Other research has revealed that porous titanium with a pore size of 200–500 μm is sufficient for adequate bone growth and fluid transport [21]. Furthermore, according to some studies, pore sizes of 300 to 800 μm and porosities of 30 to 80 vol% show reasonable performance [20]. In this sense, Chen et al. found that selective laser sintering Ti6Al4V ELI scaffolds with a pore size of 500 μm and a porosity percentage of 60 vol% showed the best results both in vitro and in vivo studies [22]. However, porous materials were observed to favor the proliferation of bacteria and, with increasing pores, a greater degree of attachment of bacteria to titanium scaffolds was produced [23].

Porous structure is another key factor in the biological and biomechanical behavior of scaffolds [10,16]. Regarding the shape of the pores, scaffolds with circular, square, hexagonal triangular, rectangular, rhomboidal, pentagonal, and heptagonal pore morphology have been reported [9,16,24,25]. Simulations using the finite element method have shown that irregular morphological pores function as stress concentrators and generate a significant increase in stress levels in scaffolds [26–28]. In addition, this may cause the scaffolds to exhibit low fatigue resistance, which may affect their clinical success. Recently, Yang et al. found that in scaffolds with triply periodic minimal surface (TPMS) and Schoen Gyroid (SG) cellular structures, the FEM can be used to predict their mechanical responses and, also, it was possible to customize their mechanical properties for different applications [29]. On the other hand, Deng et al. found that pore architecture had an influence on bone growth and obtained the best results using diamond lattice unit (DIA) between four scaffolds with different topology [16]. In other words, interconnected pores were considered to facilitate bone growth within scaffolds [18,22].

Since the parameters of the porous structures of scaffolds influence bone generation, in scaffolds for bone restoration, porosity must be controlled in terms of percentage, degree of interconnectivity, size, morphology and distribution. However, conventional manufacturing methods do not allow precise control of the percentage of porosity and the size, shape, distribution, and connectivity of pores [16]. Recent advances in the fields of medical imaging processing and additive manufacturing (AM) processes have allowed the development of customized scaffolds [10,30]. The AM or 3D printing process allows the scaffold to be manufactured in terms of shape, interconnectivity, and pore sizes, as well as variation in the mechanical properties of the material [16]. Furthermore, both the general shape and the internal structure of the scaffold can be customized with high reproducibility and reliability [30]. Among additive manufacturing techniques, electron beam melting (EBM), selective laser melting (SLM), and selective laser sintering (SLS) have been considered fast and successful methods for the manufacture of medical implants [24,31,32]. These techniques, due to their good controllability and level of precision, have a high potential for the manufacture of porous implants [24,31,32] such as metal scaffolds.

Furthermore, images of atrophied areas of the maxillae acquired by computed axial tomography (CAT) or nuclear magnetic resonance [10,30] allowed for precise three-dimensional (3D) images of atrophied areas of the jaws and their defects, while their use in AM processes allowed them to be implanted for customized bone regeneration. Customized scaffolds allow the architecture and dimensions of partially or completely edentulous jaws to be recovered, and in some cases the patient can simultaneously restore chewing function [33]. Furthermore, the placement of custom 3D printed scaffolds in atrophied maxillae can be combined with the anchoring of dental implants during a surgical operation, so a second operation can be avoided [7,33].

The evaluation of the biomechanical behavior of load bearing devices is important. In this context, overloads and underloads are known to affect the bone remodeling process and contribute to *peri*-implant bone atrophy [34]. To avoid these phenomena, the Finite Element Method (FEM) has been used in different studies to simulate the biomechanical behavior of maxillofacial devices [35–38]. Using this method, physical factors, such as mechanical stress and strain, can be calculated and illustrated [36,39]. Specifically, its use in endosseous dental implants has improved their macro-design [40,41]. Furthermore, this method has been used to evaluate the biomechanical behavior of different types of scaffolds intended for bone regeneration [31,42,43] and also to optimize the design of scaffolds for maxillofacial applications [35].

The main objective of this work was to evaluate by FEM the influence of the diameter of the holes and the porosity percentage of the custom scaffolds on stress and strain levels in a type IV bone. For this, the customized scaffolds were fixed using a dental implant in a partially edentulous jaw.

2. Materials and methods

2.1. Models

Medical images in DICOM format were used from a computerized axial tomography (CAT) of a 46-year-old partially edentulous man. Images were acquired in grayscale and distributed in different anatomical sections (axial, sagittal, and coronal). They were taken with a Siemens Sensation Cardiac 64 scanner (Siemens, Germany), with a matrix size of 512 × 512 pixels, a spatial resolution of 0.33 mm, a panoramic field of view of 48.6 cm and a spacing between slices of 0.625 mm.

CAT images were processed in Mimics Innovation Suite 17.0 software (Materialise, Leuven, Belgium). First, using the 'Thresholding' tool, a bone mask was obtained from the apparent density of bone tissue (Hounsfield scale, gray scale). Then the 'Edit Mask' and 'Calculate 3D' functions were used to refine the selected area

and obtain the 3D model of the craniomaxillofacial region of the patient (Fig. 1a), respectively. The image of the atrophied maxilla was modified to allow its export to the Autodesk Inventor 2016 mechanical design software (Autodesk Inc, USA) using tools 'Calculate polylines' and 'Cavity Fill from Polilynes'. Finally, the 3-matic tool of the Mimics software was used to smooth the maxillary surface and export it to the Inventor software in STEP format.

Table 1 summaries the dimensions of the jaw in the atrophied zone (used to obtain the design of the scaffolds) and in the non-atrophied zone of the patient for comparison. The absence of mechanical stimuli caused a decrease in jaw height compared to the zone supporting the canines and incisors (non-atrophic zone).

By using the software Inventor, an edentulous jaw segment with a bone quality IV (Fig. 1b), according to the Lekholm and Zarb classification [44] was obtained. A threaded hole (Fig. 1b) was made in the jaw segment for the anchorage of a dental implant (with a profile of its threads that corresponds to those of that implant (Fig. 3a)) and customized scaffolds were also designed (Fig. 2). From the model of the atrophied jaw segment, the architecture and cellular structure of the scaffolds were obtained in the software Inventor. In the first design stage, a dense model was obtained (Fig. 2a), as previously reported [45]. Three-dimensional interconnected cylindrical holes with a previously selected diameter and porosity percentage were incorporated into the scaffolds, forming the cellular structure and the periodic cellular unit shown in Fig. 2b. This structure was characterized by struts of variable thickness and sharp edges, as well as a cubic cell and a minimal strut size (MSS) as shown in Table 2. Porosity was obtained by incorporating a hole in the axial direction (y-axis) of the dense model. Then, using the "Pattern" tool, holes were placed on its surface. This process was repeated in the mesiodistal and buccolingual directions. In all three directions, a distance was kept between the holes that maintained the porosity level selected for each experimental run. Finally, a hole with a conical area and another threaded area was added for the placement of the dental implant (Fig. 2c).

Furthermore, in Inventor software, the crown was assembled to the dental implant and the dental implant was anchored to the jaw (Fig. 3a). To assemble the system components, they were converted to the SAT format and then exported as independent pieces to the Abaqus CAE software. A detailed explanation of the processing of CT images, obtention of the 3D model of the maxilla, exporting the model from the Mimic software to the Inventor software, as well as the obtaining of the dense model of personalized scaffolds was reported in a previous work [45].

Table 1
Dimensions of the jaw.

Parameter	Jaw dimensions (mm)	
	Atrophied	Non-atrophied
Minimum height	23	27
Maximum height	27.6	30.1
Minimum thickness	14	12.5*
Maximum thickness	16.8	13.9

* The lower thickness values in the non-atrophic zone were probably influenced by the fact that in this zone the canines and incisors were located.

The customized crown-dental implant scaffold system used in the simulations is shown in Fig. 3a. To form the evaluated system, a new single-component dental implant model was chosen characterized by having a length of 12 mm (threaded area), a tapered thread, a neck diameter of 3.8 mm, and a second thread in the proximal area (close to the neck). The threads presented the following characteristics: rectangular profile, 1.2 mm pitch, variable thread height (0.6 mm in the apical zone and approximately 0.2 mm in the proximal zone) and a width of 0.3 mm. The scaffold was placed and fixed to the jaw by the dental implant in such a way that its movements in all directions were limited.

2.2. Three-dimensional finite element analysis

The system (Fig. 3a) was exported to Abaqus / CAE software (6.13 version, Simulia Corp.) to simulate it using FEM, considering that living tissues adapt to mechanical loads. To evaluate the behavior of bone systems, the von Mises equivalent stress criterion was used. Furthermore, the von Mises strain was used to assess the behavior of the cortical and trabecular bones. An experimental design was obtained in StatGraphics Centurion 19, in which the scaffolds were assigned three diameters to their holes and three values of the porosity percentage (Table 2). The levels of both variables were selected from the results reported in different studies [20,22,46]. Maximum values of von Mises equivalent stress (MVMES) and von Mises strain (MVMS) were evaluated as response variables, both in the cortical *peri*-implant bone and in the trabecular bone. The distribution of these variables along the *peri*-implant bone was also obtained.

The Ti6Al4V alloy was used in both the design of the scaffolds and the dental implant, while a feldspathic ceramic was used in

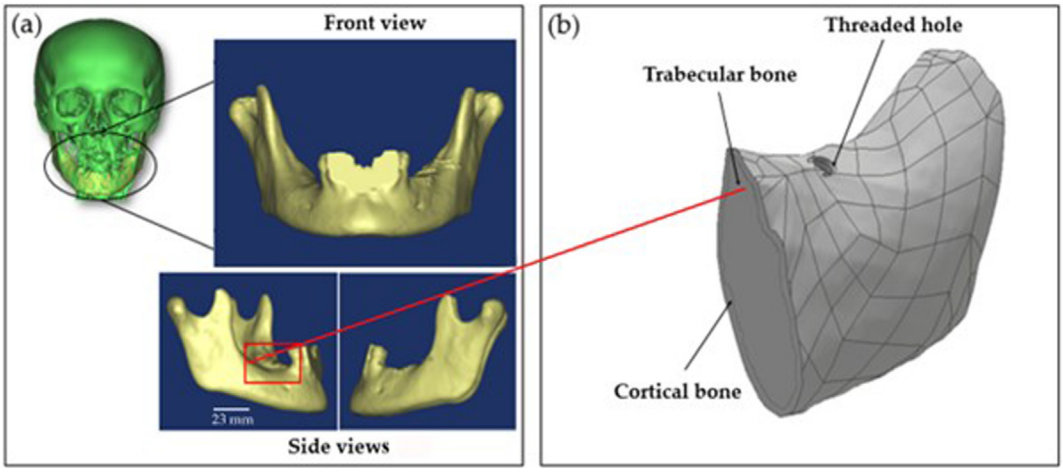

Fig. 1. (a) Craniomaxillofacial region and partially edentulous jaw of the patient and (b) jaw segment used in the FEM simulations.

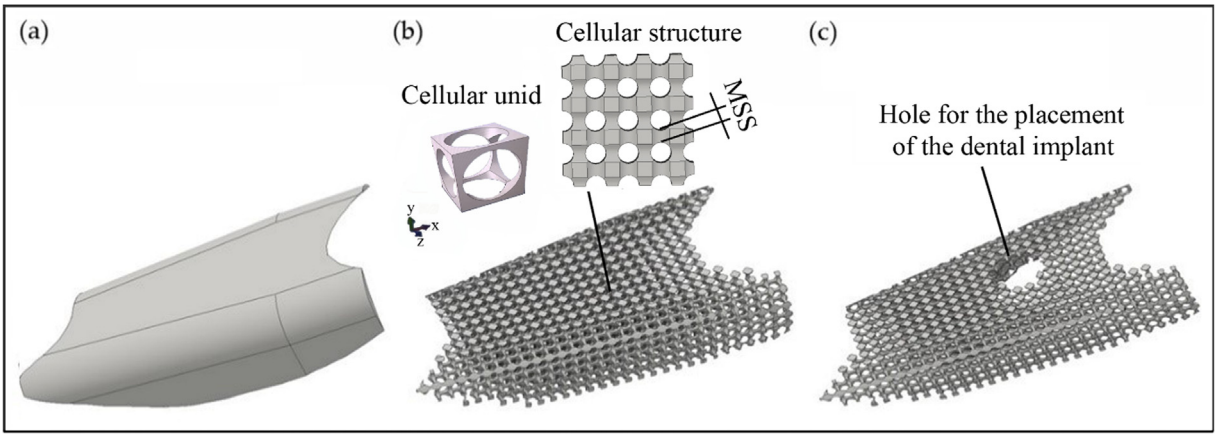

Fig. 2. Models generated during the design stages of customized scaffolds: (a) solid model, (b) porous scaffold and its cellular structure, and (c) porous scaffold with a hole for the placement of the dental implant.

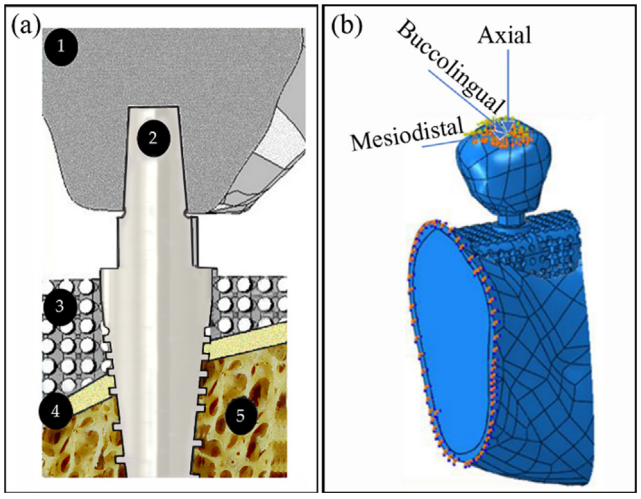

Fig. 3. Simulated systems and load conditions. (a) Schematic representation of the cross section of the simulated system, where: (1) crown, (2) dental implant, (3) customized scaffold, (4) cortical bone, and (5) trabecular bone. (b) Boundary conditions, load location (nodes where the load was distributed) and load directions.

the crown. Table 3 shows the values of the mechanical properties assigned to the different components of the evaluated systems. All materials were assumed to be linearly elastic and isotropic, since all volumes of materials were considered homogeneous.

Table 3
Mechanical properties of the materials used in the simulated runs.

Materials	Young's modulus (MPa)	Poisson ratio
Cortical bone* [47]	13,000	0.30
Trabecular bone* [47]	690	0.30
Feldspathic ceramics [48]	82,800	0.35
Ti6Al4V dense [49,50]	110,000	0.32
Ti6Al4V with porosity of 45 % [51,52] porosity	22,000	0.32
Ti6Al4V with 65 % porosity [52]	7000	0.32
Ti6Al4V with 80 % porosity [51]	5000	0.32

* Type IV bone quality.

To evaluate the models, the systems were subjected to static loads and the interactions between parts of the assembly were defined as a tie-type (delayed load condition, complete osseointegration between implants and bone tissues), using the load values reported by Himmlova et al. (in the axial direction: 114.6 N, in the mesiodistal direction: 23.4 N and in the buccolingual direction: 17.1 N) [53]. These loads were assumed to act on the surface of the crown, generating forces that are transmitted to the rest of the system. Similarly, a set of 40 nodes (colored areas in Fig. 3b) was created in the upper area of the crown, where the loads were distributed, representing its application at an angle of 75° with the occlusal plane. The boundary conditions used restrict the degrees of freedom in the x, y, and z directions and can also be seen in Fig. 3b.

Tetrahedral elements corresponding to the C3D10 type element from the Abaqus element library were used in the models. To

Table 2
Experimental design used and scaffold parameters.

Model	Scaffold Parameters			
	Hole diameter (μm)	Porosity vol. (%)	MSS* (μm)	Cellular size (μm)
A	350	45	330	680
B	550	80	120	670
C	350	65	180	530
D	550	65	300	850
E	350	80	70	420
F	750	45	620	1370
G	750	80	130	880
H	550	45	680	1230
I	750	65	430	1180

* Minimum strut size.

reduce the computing capacities to be used, the system was meshed in a global and refined way (local mesh, with a smaller element size) in the areas where the dental implant - maxillary bone and scaffold - maxillary bone contact occurs. After convergence analysis, the local and global mesh sizes were assigned 0.16 and 0.11, respectively. To perform the convergence analysis, the model with 350 μm diameter and 65 vol% porosity percentage was selected. Four local meshes with different amounts of elements were made, whose values vary from approximately $1{\cdot}6 \times 10^6$ – $4{\cdot}3 \times 10^6$, using the same loading and boundary conditions. The selected local mesh was 0.11 mm as shown in Table 4 (difference less than 2 % of the MEVMS compared to the next run).

2.3. Statistical analysis

In the Abaqus/CAE software, the most loaded nodes of the areas with the highest level of stress were determined in the cortical and trabecular bones. Data were processed in StatGraphics Centurion 19 software (Statpoint Technologies, Warrenton, VA, USA) and the stress range of the most loaded zones was expressed as mean ± standard deviation. Multiple sample comparison tests (multiple-range tests, Tukey HSD) were used to determine the existence of significant differences between the groups for a normal population distribution and a Kruskal-Wallis test for a non-normal population distribution. A value of $p < 0.05$ was taken as a statistically significant difference.

3. Results and discussion

Different authors have already reported on FEM studies of scaffolds for bone applications [10,31,54–56]. It made it possible to optimize its architecture and thereby improve its mechanical properties and in vivo behavior. Different parameters (shape, size and interconnection of pores and porosity percentage), as well as response variables such as mechanical properties, permeability and cell response were evaluated [10,26,31,57]. The regeneration of atrophied jaws and, in some cases, with the simultaneous restoration of patient masticatory function were among the applications of these devices [33]. It could be achieved using scaffolds fixed with dental implants. However, the evaluation of the biomechanical behavior of scaffolds fixed by dental implants in the maxilla is a current problem.

Mechanical stimuli were known to improve the bone remodeling process. Both stress and strain were factors that influence the bone remodeling process [18,34,58], although overload or underload can affect implant osseointegration and *peri*-implant bone density [34]. Overloaded endosseous implants can cause premature failure and compromise their clinical success. In the first stage of this work, the distribution and maximum values of stresses generated in the crown, dental implant, and personalized scaffolds were evaluated from nine experimental runs. Subsequently, the research focused on the evaluation of the influence of the hole diameter and the porosity percentage of the scaffolds on the stress and strain distribution in *peri*-implant bone. Furthermore, the MVMES and MVMS values were obtained in the cortical and trabecular bones.

Table 4
Convergence analysis for a system with a scaffold model corresponding to the experimental run C.

Run number	Elements sizes	Total of elements	MEVMS (MPa)
1	0.16	1 610 307	21.90
2	0.12	2 400 270	22.88
3	0.11	3 038 316	23.33
4	0.09	4 314 408	23.72

3.1. Distribution of von Mises equivalent stress in crown, dental implant, and customized scaffolds

The highest levels of von Mises equivalent stress in the crown and dental implant were concentrated in the area where both contacts (corresponding to the prosthetic support of the dental implant) (Fig. 4 a, c). In the scaffold, the maximum values were in its upper zone, mainly in areas (in the struts) close to the neck of the dental implant (Fig. 4b). This behavior was similar to that generated by the rest of the experimental runs.

Fig. 5 shows the MVMES generated by the nine simulated experimental runs in the crown (Fig. 5a), dental implant (Fig. 5b) and customized scaffolds (Fig. 5c). In the crown, stress values of less than 35 MPa were obtained. In the case of dental implants, values of less than 300 MPa were obtained, which were significantly lower than the yield strength of the implant material (1000–1250 MPa in the Ti6Al4V, depending on the fabrication parameters by selective laser melting (SLM) and a post-heating treatment) [59]. It should be noted that in systems with scaffolds that present 80 vol% porosity percentage, the dental implant showed the highest values of MVMES, a result that may be related to a lower transmission of loads to the porous scaffold. In addition, in general, a decrease in the MVMES values was obtained in the scaffolds as the percentage and diameter of the holes increased. These atypical results could be explained by considering that the scaffolds are part of a system that supports and transmits the applied loads. In this context, the scaffold received a lower load from the dental implant (Fig. 5b) and, at the same time, a higher load is transmitted to the *peri*-implant cortical bone (reducing the phenomenon of stress-shielding) (Fig. 7a). On the other hand, in the scaffolds, MVMES values were obtained that did not exceed 20 MPa (Fig. 5c). In general, the MVMES values observed in the crown, scaffold and dental implant should not affect their performance under static load, considering that the MEVMS levels are significantly lower than the yield strength of its corresponding materials. However, implants for dental applications are well known to work under cyclical loads [60]. In this sense, fatigue strength was fundamental to ensure the long-term performance of dental devices [56]. Specifically, scaffolds were found to have low fatigue resistance, which depended, among other factors, on their structural design pores, unit cell type, as well as on their porosity and the post-manufacturing processes to which they were subjected [56]. Therefore, it would be recommended to simulate the system under dynamic loads and perform fatigue compression tests on the scaffolds. It could also be suggested to consider failures due to cyclic fatigue, associated with wrong material selection and/or implant design. In fact, it is well-known that fatigue strength in 10^7 cycles presented values 27–35 MPa and 200–430 MPa for cortical bone and commercially pure titanium implants (obtained by a forging process), respectively [61]. Considering this fact, it would be highly recommended for future works to implement models that estimate the fatigue behavior of the implant and the customized scaffolds proposed in this work.

3.2. Distribution of von Mises equivalent stress and von Mises strain in the cortical and trabecular bones

In general, to evaluate the equivalent von Mises stress and von Mises strain in the cortical and trabecular bones, the maximum values of both parameters were chosen because they had a greater influence on the in vivo behavior of implantable dental devices. The stress distribution in the cortical bone by the experimental runs of the system is shown in Fig. 6a. In all simulated experimental runs, the MVMES values in the cortical bone were concentrated in the area in contact with the threads of the dental implant.

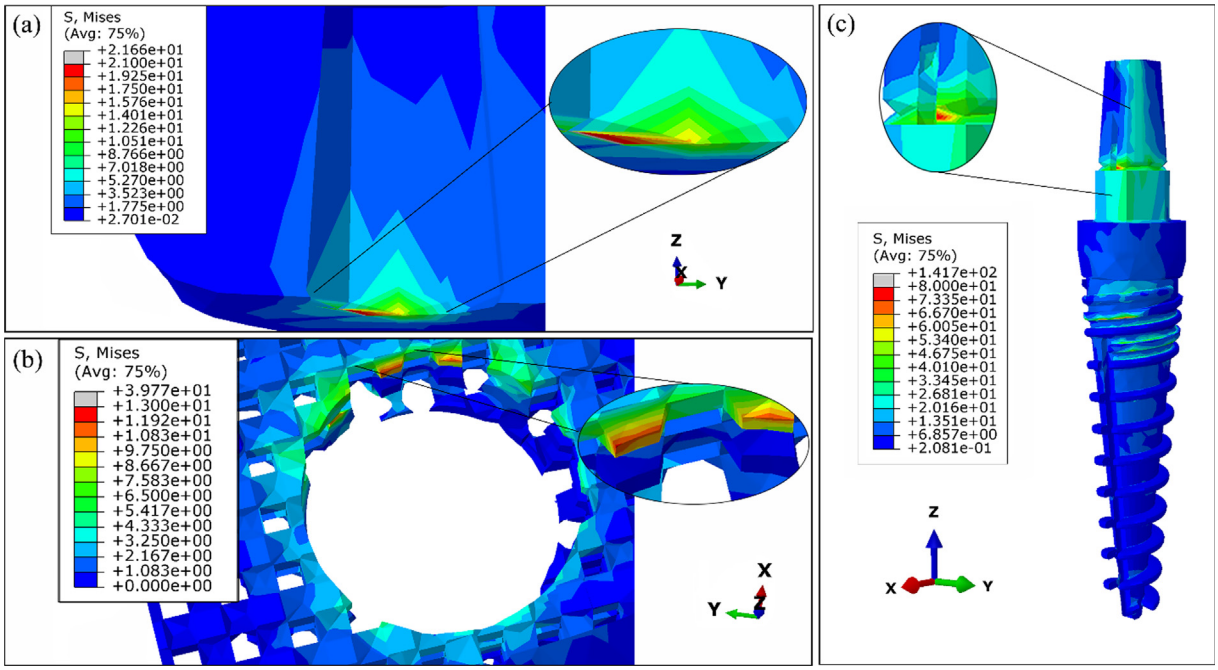

Fig. 4. Distribution of von Mises stress generated by the experimental run D (central point of the experimental design): (a) crown (cross section), (b) scaffold and (c) dental implant.

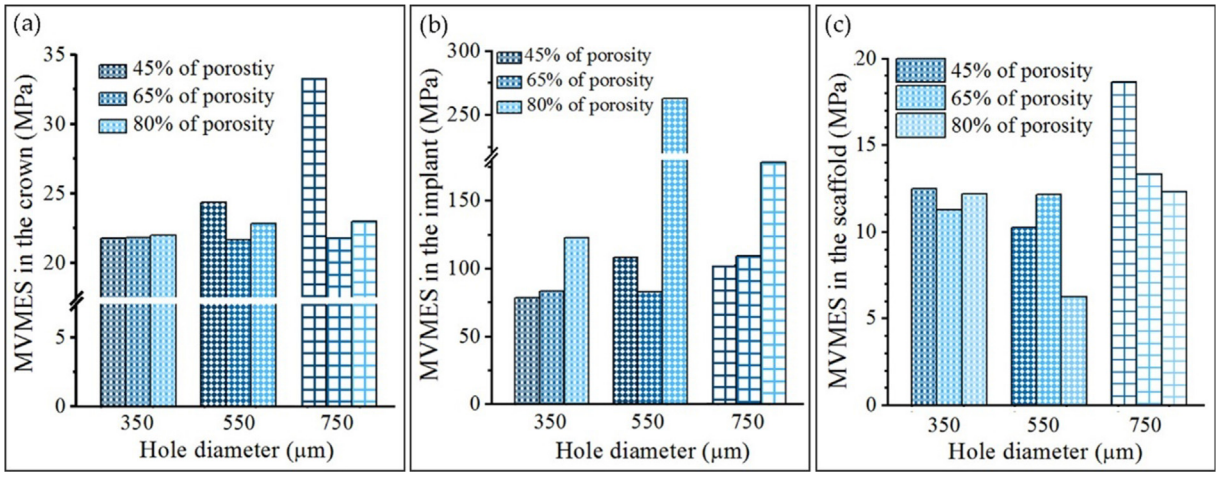

Fig. 5. Influence of hole diameter and porosity percentage of scaffolds on MVMES values for (a) crown, (b) dental implant and (c) scaffolds.

MVMES in the trabecular bone was concentrated in its *peri*-implant area in contact with the apical region of the dental implant and at its interface with the cortical bone (Fig. 6c). Furthermore, stress levels in the *peri*-implant bone throughout the implant body were similar, although significant differences were observed when comparing their values at the buccal, lingual, mesial, and distal sites. This behavior could be related to the application of an oblique load.

Fig. 6b and 6d show the distribution of the strains generated by the experimental run D in the cortical and trabecular bones. In general, these distributions were representative of the rest of the simulated runs. The highest strain values in both bones were concentrated in areas similar to those of stress, a result expected. In all runs, the highest von Mises strain values were observed in the area in contact with the threads of the dental implant. In the case of the trabecular bone, they were observed in small regions close to their interface with the cortical bone. Furthermore, an asymmetric distribution of strains was observed in the *peri*-implant bone (higher values on the left side of the dental implant in Fig. 6d). However, this behavior must vary when changing the direction of the load.

3.3. Effect of the diameter of the hole and the percentage of scaffold porosity on MVMES and MVMS in the peri-implantar bone

Generally, the MVMES values obtained were lower than those reported for human bones. In this sense, the compressive strength of human cortical bone ranges 90–230 MPa, while that of cancellous bone ranges 2–45 MPa [62]. On the other hand, several studies suggested that high stress values can lead to *peri*-implant bone absorption, even causing bone loss and implant failure [5,34,58,63,64]. In general, MVMES values between 10 and 28 MPa were obtained in the cortical bone, while the experimental runs F and G generated the highest values (Fig. 7a). MVMES values

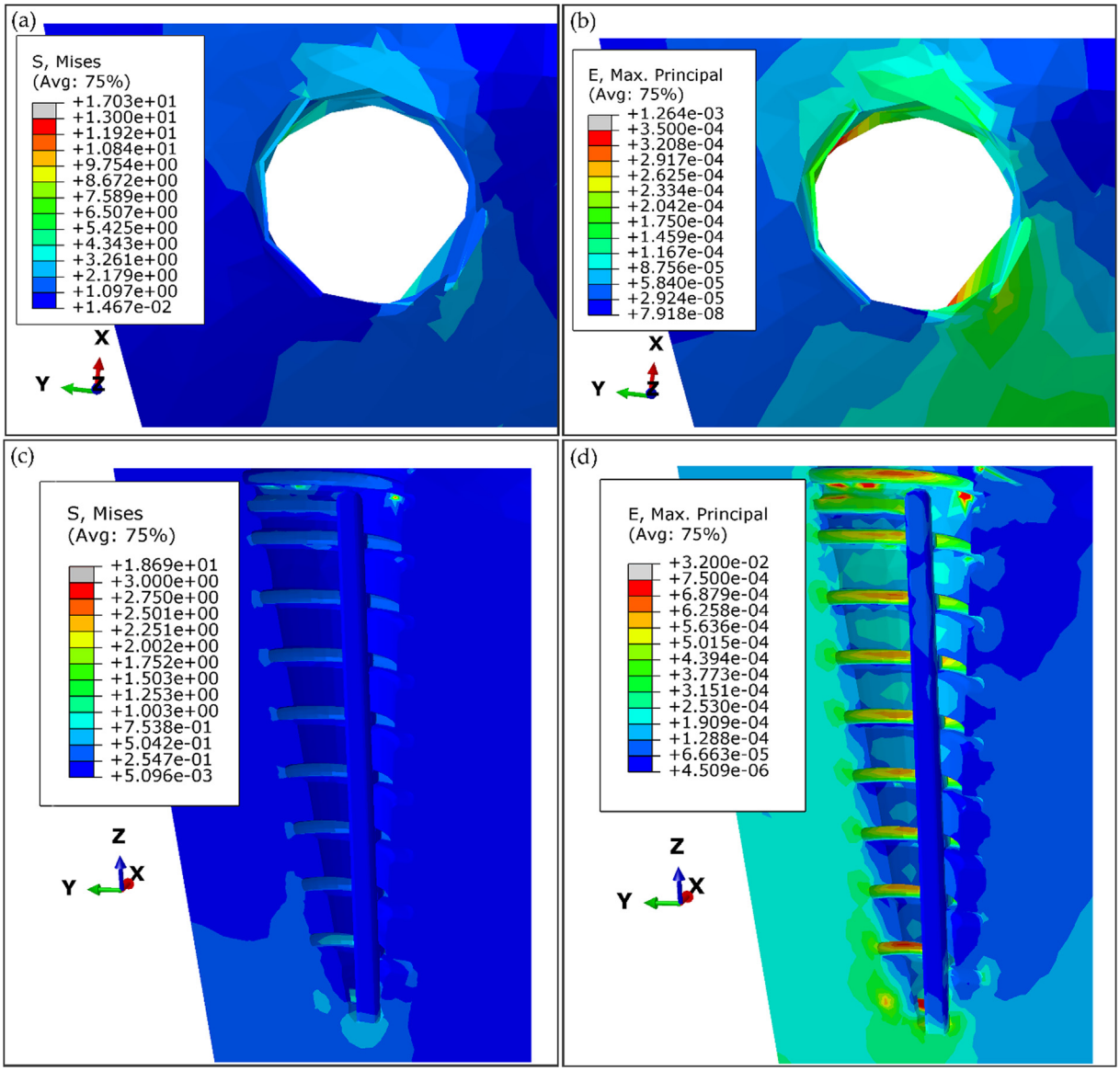

Fig. 6. (a) Distribution of von Mises equivalent stress in cortical bone, (b) distribution of von Mises strain in cortical bone, (c) distribution of von Mises equivalent stress in trabecular bone, and (d) distribution of von Mises strain in trabecular bone generated by experimental run D (central point of the experimental design).

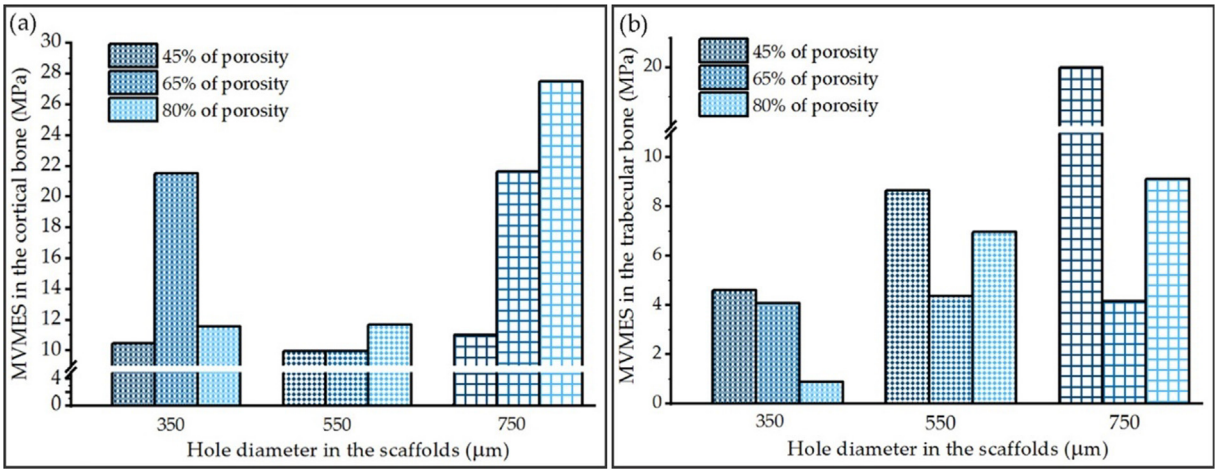

Fig. 7. MVMES values, (a) in the cortical bone and (b) in the trabecular bone.

were within the range recommended by Li et al. to avoid overloading in the cortical bone [34]. The range of stresses necessary to obtain adequate bone remodeling was a function of bone (cortical or trabecular) and also of jawbone quality at the implantation site (type I, II, III, or IV). For example, according to Li et al. for cortical bone with a density of 1.8 g/cm^3 (density used in the simulations) it was approximately between 12 and 28 MPa [34]. Stress values were lower than those observed with dental implants evaluated in a previous study [39], as well as those reported in different studies when using different models of endosseous dental implants [40,53]. Furthermore, the results of variants with a hole diameter of 750 μm of the scaffold corroborated the effect of increasing the percentage of scaffold porosity on the decrease in shielding stresses. In the trabecular bone, MVMES values between 1 and 20 MPa were obtained and their maximum levels were also generated by the experimental runs F and G (Fig. 7b). In some cases, these values were higher than those recommended for bone quality IV (approximately between 1.5 MPa and 4.2 MPa for a bone density of 0.65 g/cm^3) [34]. However, the area they occupied was generally small and their levels were lower than those reported for this bone quality [40].

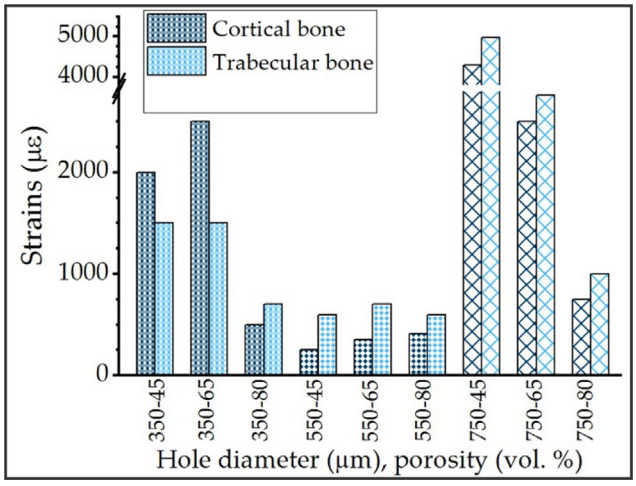

Fig. 8. MVMS values in the cortical and trabecular bone generated by the experimental runs.

Fig. 8 shows the MVMS values in the *peri*-implant bone. The strain values in the cortical and trabecular bones were generally observed to not exceed 3000 με (strains × 10^{-6}), except for the experimental run F. Furthermore, small areas in the *peri*-implant bone were observed in which the strain values are lower than 100 με, that can cause bone disuse [65,66], which could result in loss of bone density and mass [58]. MVMS values were generally higher in the trabecular bone, a behavior that could be related to the low density assigned to this bone and the lower influence of the scaffolds in this area.

In general, the obtained MVMS values (between 300 and 3000 με) were considered adequate for the processes of bone growth, bone remodeling, or bone density maintenance. A sufficient transfer of load to the *peri*-implant bone tissue was considered a key factor in the long-term success of endosseous implants [40]. There was a consensus that bone strain values ranging from 100 to 3000 με do not affect the *peri*-implant bone density [18,65,66]. When bone strain is less than 100 με, it will lead to absorption of bone disuse [18]. On the other hand, strains above 3000 με were considered problematic for bone, leading to a hypertrophic response, while levels of bone strains above 4000 με could cause local overload and bone loss in affected areas [53].

The influence of the variables studied on the MVMES values is shown in Fig. 9a and 9b, while its influence on the MVMS is shown

Table 5
Statistically significant differences in the stress range of the most loaded zones in the cortical and trabecular bone between the experimental runs.

Experimental run	Statistically significant differences with	
	Cortical bone	Trabecular bone
A (350–45)*	C, D, E, G, H, I	B, E, G, F, H
B (550–80)	C, E, G, H, I	A, C, D, E, F, I
C (350–65)	A, B, D, F, H,	B, E, F, G, H, I
D (550–65)	A, C, E, F, G, I	B, E, F, G, H
E (350–80)	B, D, G, H, I	A, B, C, D, F, G, H, I
F (750–45)	A, C, D, G, H, I	A, B, C, D, E, H, I
G (750–80)	A, B, D, E, F, H	A, C, D, E, I
H (550–45)	A, B, C, E, F, G, I	A, C, D, E, F, I
I (750–65)	A, B, D, E, F, H	B, E, H, G, F

* First number: diameter of the hole diameter (μm), second number: porosity of the scaffold (vol.%).

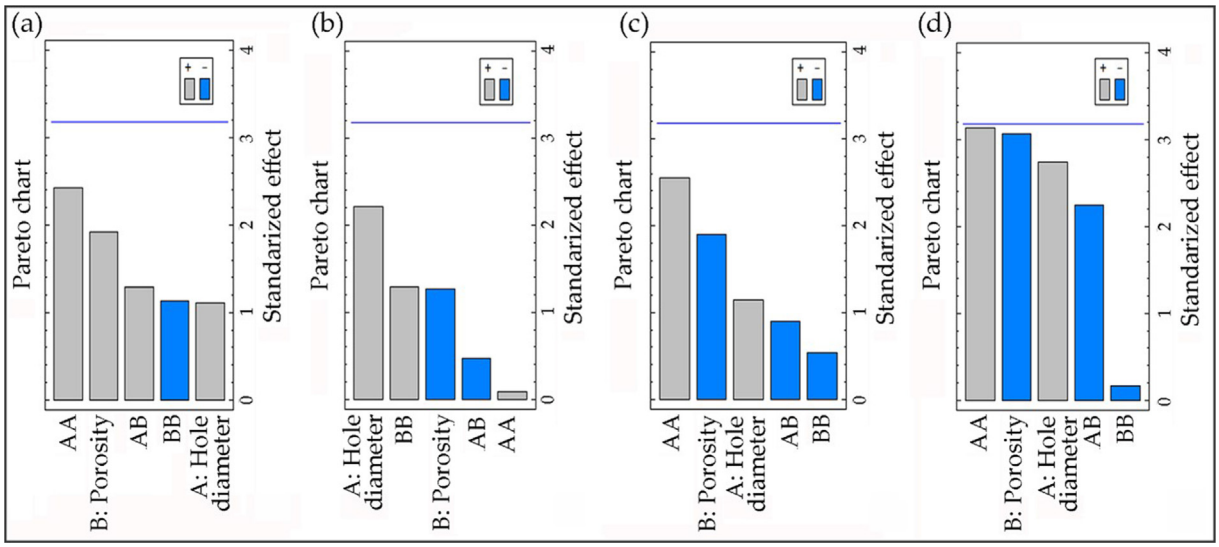

Fig. 9. Influence of on the MVMES values (a and b) and the MVMS values (c and d). (a) and (c) in the cortical bone (b) and (d) in the trabecular bone.

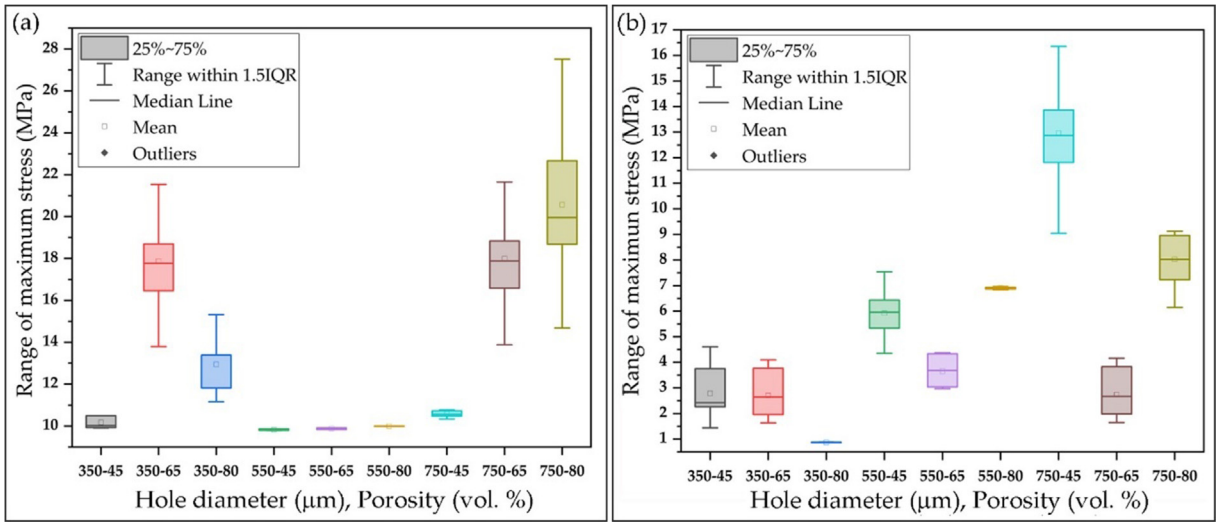

Fig. 10. Stress range in the zones most loaded in cortical bone (a) and stress range in the zones most loaded in trabecular bone (b).

in Fig. 9c and 9d. In general, the evaluated variables did not show statistically significant influence on both response variables. However, it was found that the increase in the scaffold porosity values produced an increase in the MVMES values in the *peri*-implant cortical bone, although this behavior was not observed in the trabecular bone. However, the three variants with a hole diameter on the scaffolds of 550 μm did not show this behavior, as they had similar levels of MVMES. This could probably be the reason why the porosity variable did not show a statistically significant influence on the MVMES values (Fig. 9a). However, the increase in the percentage of scaffold porosity generated a slight decrease in the MVMS values in the cortical bone, while its values in the trabecular bone were close to showing a statistically significant influence and produced a reduction in this parameter. Furthermore, an increase in the diameter of the hole was shown to produce a slight increase in the influence of both response variables in a positive way.

It is well-known that the highest stress values are not concentrated at a point in the *peri*-implant bone [40,67] and that in the overloaded area, osseointegration and bone density could be affected. Therefore, in the present work, the stress values of the zones most loaded in the cortical and trabecular bone were compared (Table 5). Fig. 10a and b show the stress range of the most loaded zones in the cortical and trabecular bone. In both cases, a correspondence was found with the MVMES values shown by the nine simulated runs (Fig. 7a and 7b). Furthermore, it was determined that the experimental variant G had the highest stress range in the cortical bone and statistically significant differences from the rest of the variants, except for runs C and I (Table 5). In the trabecular bone, the highest value of the stress range of the most loaded zones was shown by the experimental run F. This range presented statistically significant differences with the rest of the experimental runs, except for G. However, the runs that had the lowest stress intervals in the cortical bone were D and H (with statistical differences from the A, C, E, F, G, I runs and A, B, C, E, F, G, I runs respectably). In the trabecular bone, run E showed the lowest stress range with statistically significant differences with the rest of the experimental runs.

In general, the experimental run I (with a hole diameter of 750 μm and 65 vol% porosity) presented the best biomechanical behavior. However, the values of MVMES and MVMS were generally confined to small areas. Therefore, it was recommended to determine the *peri*-implant bone area, generated by the experimental runs, which was within the recommended ranges of both variables to maintain bone density. Furthermore, mechanical tests under static and dynamic compression loads and in vitro and in vivo biological tests were necessary for a complete evaluation of the scaffolds.

4. Conclusions

Through medical image processing, a three-dimensional model of an edentulous jaw segment with IV bone quality was obtained, which presented atrophy. On the basis of this model, the design of the customized scaffolds was performed in such a way that it allows recovery of the dimensions and architecture of the jaw segment. In addition, customized scaffolds fixed by a dental implant were modeled to restore the patient's chewing function. Simulation of those systems using FEM allowed to evaluate their biomechanical behavior. The MVMES values obtained in the crown, dental implant, and scaffolds should not affect their performance under static loads.

It was determined that the use of scaffolds fixed by a dental implant produces a decrease in the stresses and strains generated in the *peri*-implant bone compared to that obtained using the traditional system of dental implants. This particular behavior was observed in the upper region of the jaw segment (cortical bone), an area that is generally the most loaded when endossoeus dental implants were used. Furthermore, it was found that the simulated variables and their interactions do not show a statistically significant influence on MVMES and MVMS in the *peri*-implant bone. However, an increase in the porosity percentage of the scaffolds was shown to produce a slight increase in the MVMES values in the cortical bone and a decrease in its levels in the trabecular bone. Furthermore, it was determined that some experimental runs generated significantly higher levels in the stress range presented by the most loaded zones. In this sense, runs G and F showed the highest stress levels in the cortical and trabecular bone, respectively. On the other hand, the lowest values were presented by runs D and H (in the cortical bone) and E (in the trabecular bone). Furthermore, higher porosity percentage values produced decreases in MVMS values in both bones, which were higher and close to showing a statistically significant influence on the trabecular bone. In general, the biomechanical behavior obtained indicates that the scaffolds should exhibit adequate performance in vivo.

CRediT authorship contribution statement

Jessica León de Ulloa: Conceptualization, Project administration, Supervision, Methodology, Investigation, Formal analysis, Val-

idation, Writing – original draft. **Jesús E. González:** Project administration, Writing - original draft, Writing - review & editing. **Ana M. Beltrán:** Investigation, Formal analysis, Validation, Writing - original draft, Writing - review & editing. **Eduardo Peón Avés:** Conceptualization, Project administration, Supervision, Methodology, Writing – original draft. **Jennifer Rodríguez-Guerra:** Investigation, Formal analysis, Validation, Writing – original draft. **Yadir Torres:** Conceptualization, Project administration, Supervision, Methodology, Writing – original draft.

Data availability

The data that has been used is confidential.

Declaration of Competing Interest

The authors declare that they have no known competing financial interests or personal relationships that could have appeared to influence the work reported in this paper.

Acknowledgement

This publication is part of the R + D + i project PID2019-109371 GB-I00, financed by MCIN/ AEI/10.13039/501100011033/. This work was also performed in the frame of the project "Personalized biomedical devices for bone and orthopedic restoration through 3D Printing" (PN385LH007-036) of the Cuban National Science and Technology program: Biotechnology, Pharmaceutical Industry, and Medical Technologies.

Data availability

The raw data required to reproduce these findings cannot be shared at this time as the data also forms part of an ongoing study. The processed data required to reproduce these findings cannot be shared at this time as the data also forms part of an ongoing study.

References

[1] M. Toledano-Osorio, M. Toledano, F.J. Manzano-Moreno, C. Vallecillo, M. Vallecillo-Rivas, A. Rodriguez-Archilla, R. Osorio, Alveolar bone ridge augmentation using polymeric membranes: A systematic review and meta-analysis, Polymers 13 (7) (2021) 1172.
[2] B.S. McAllister, K. Haghighat, Bone augmentation techniques, J. Periodontol. 78 (3) (2007) 377–396.
[3] L. Polo-Corrales, M. Latorre-Esteves, J.E. Ramirez-Vick, Scaffold design for bone regeneration, J. Nanosci. Nanotechnol. 14 (1) (2014) 15–56.
[4] L. Tettamanti, M.A. Bassi, G. Trapella, V. Candotto, A. Tagliabue, Applications of biomaterials for bone augmentation of jaws: Clinical outcomes and in vitro studies, Oral Implantol. 10 (1) (2017) 37.
[5] S. Nimbalkar, P. Dhatrak, C. Gherde, S. Joshi, A review article on factors affecting bone loss in dental implants, Mater. Today: Proc. 43 (2021) 970–976.
[6] P. Rider, Ž. Kačarević, S. Alkildani, S. Retnasingh, R. Schnettler, M. Barbeck, Additive manufacturing for guided bone regeneration: A perspective for alveolar ridge augmentation, Int. J. Mol. Sci. 19 (11) (2018) 3308.
[7] H.-J. Jeong, S.-J. Gwak, K.D. Seo, S. Lee, J.-H. Yun, Y.-S. Cho, S.-J. Lee, Fabrication of three-dimensional composite scaffold for simultaneous alveolar bone regeneration in dental implant installation, Int. J. Mol. Sci. 21 (5) (2020) 1863.
[8] I. Denry, L.T. Kuhn, Design and characterization of calcium phosphate ceramic scaffolds for bone tissue engineering, Dent. Mater. 32 (1) (2016) 43–53.
[9] H.-K. Lim, M. Ryu, S.-H. Woo, I.-S. Song, Y.-J. Choi, U.-L. Lee, Bone Conduction Capacity of Highly Porous 3D-Printed Titanium Scaffolds Based on Different Pore Designs, Materials 14 (14) (2021) 3892.
[10] M. Bahraminasab, Challenges on optimization of 3D-printed bone scaffolds, Biomed. Eng. Online 19 (1) (2020) 1–33.
[11] L. Bai, Y. Xu, X. Chen, L. Xin, J. Zhang, K. Li, Y. Sun, Improved mechanical properties and energy absorption of Ti6Al4V laser powder bed fusion lattice structures using curving lattice struts, Mater. Des. 211 (2021) 110140.
[12] Y. Dong, J. Tang, D. Wang, N. Wang, Z. He, J. Li, D. Zhao, M. Yan, Additive manufacturing of pure Ti with superior mechanical performance, low cost, and biocompatibility for potential replacement of Ti-6Al-4V, Mater. Des. 196 (2020) 109142.
[13] S. Chen, J. Huang, C. Pan, C. Lin, T. Yang, Y. Huang, C. Ou, L. Chen, D. Lin, H. Lin, Microstructure and mechanical properties of open-cell porous Ti-6Al-4V fabricated by selective laser melting, J. Alloy. Compd. 713 (2017) 248–254.
[14] N. Kamboj, A. Ressler, I. Hussainova, Bioactive Ceramic Scaffolds for Bone Tissue Engineering by Powder Bed Selective Laser Processing: A Review, Materials 14 (18) (2021) 5338.
[15] W.-T. Wang, R.-N. Sheng, Z.-L. Jhuang, Design, Test and FEM Analysis of Customized Titanium Alloy Implant with Scaffold Based on Additive Manufacturing, in: IOP Conference Series: Materials Science and Engineering, IOP Publishing, 2021, pp. 1–8.
[16] F. Deng, L. Liu, Z. Li, J. Liu, 3D printed Ti6Al4V bone scaffolds with different pore structure effects on bone ingrowth, J. Biol. Eng. 15 (1) (2021) 1–13.
[17] A.-M. Băbțan, D. Timuș, O. Soriță, B.A. Boșca, R. Barabas, A. Ionel, N.B. Petrescu, C.N. Feurdean, I.R. Bordea, G. Saraci, Tissue integration and biological cellular response of SLM-manufactured titanium scaffolds, Metals 10 (9) (2020) 1192.
[18] T. Liu, Y. Chen, A. Apicella, Z. Mu, T. Yu, Y. Huang, C. Wang, Effect of porous microstructures on the biomechanical characteristics of a root analogue implant: An animal study and a finite element analysis, ACS Biomater. Sci. Eng. 6 (11) (2020) 6356–6367.
[19] S. Barui, S. Chatterjee, S. Mandal, A. Kumar, B. Basu, Microstructure and compression properties of 3D powder printed Ti-6Al-4V scaffolds with designed porosity: Experimental and computational analysis, Mater. Sci. Eng., C 70 (2017) 812–823.
[20] J. Wo, S.-S. Huang, D.-Y. Wu, J. Zhu, Z.-Z. Li, F. Yuan, The integration of pore size and porosity distribution on Ti-6Al-4V scaffolds by 3D printing in the modulation of osteo-differentation, J. Appl. Biomater. Funct. Mater. 18 (2020) 2280800020934652.
[21] Z.J. Wally, W. Van Grunsven, F. Claeyssens, R. Goodall, G.C. Reilly, Porous titanium for dental implant applications, Metals 5 (4) (2015) 1902–1920.
[22] Z. Chen, X. Yan, S. Yin, L. Liu, X. Liu, G. Zhao, W. Ma, W. Qi, Z. Ren, H. Liao, Influence of the pore size and porosity of selective laser melted Ti6Al4V ELI porous scaffold on cell proliferation, osteogenesis and bone ingrowth, Mater. Sci. Eng., C 106 (2020) 110289.
[23] A. Civantos, A.M. Beltrán, C. Domínguez-Trujillo, M.D. Garvi, J. Lebrato, J.A. Rodríguez-Ortiz, F. García-Moreno, J.V. Cauich-Rodriguez, J.J. Guzman, Y. Torres, Balancing porosity and mechanical properties of titanium samples to favor cellular growth against bacteria, Metals 9 (10) (2019) 1039.
[24] F. Liu, Q. Ran, M. Zhao, T. Zhang, D.Z. Zhang, Z. Su, Additively manufactured continuous cell-size gradient porous scaffolds: pore characteristics, mechanical properties and biological responses in vitro, Materials 13 (11) (2020) 2589.
[25] F.N. Habib, M. Nikzad, S.H. Masood, A.B.M. Saifullah, Design and development of scaffolds for tissue engineering using three-dimensional printing for bio-based applications, 3D Printing Add. Manuf. 3 (2) (2016) 119–127.
[26] S. Lascano, C. Arévalo, I. Montealegre-Melendez, S. Muñoz, J.A. Rodriguez-Ortiz, P. Trueba, Y. Torres, Porous titanium for biomedical applications: Evaluation of the conventional powder metallurgy frontier and space-holder technique, Appl. Sci. 9 (5) (2019) 982.
[27] S.M. Castillo, S. Muñoz, P. Trueba, E. Díaz, Y. Torres, Influence of the Compaction Pressure and Sintering temperature on the mechanical properties of porous titanium for biomedical applications, Metals 9 (12) (2019) 1249.
[28] L. Bai, C. Gong, X. Chen, J. Zheng, L. Xin, Y. Xiong, X. Wu, M. Hu, K. Li, Y. Sun, Quasi-Static compressive responses and fatigue behaviour of Ti-6Al-4 V graded lattice structures fabricated by laser powder bed fusion, Mater. Des. 210 (2021) 110110.
[29] L. Yang, C. Yan, C. Han, P. Chen, S. Yang, Y. Shi, Mechanical response of a triply periodic minimal surface cellular structures manufactured by selective laser melting, Int. J. Mech. Sci. 148 (2018) 149–157.
[30] C. Garot, G. Bettega, C. Picart, Additive manufacturing of material Scaffolds for bone regeneration: toward application in the clinics, Adv. Funct. Mater. 31 (5) (2021) 2006967.
[31] X.-Y. Zhang, G. Fang, J. Zhou, Additively manufactured scaffolds for bone tissue engineering and the prediction of their mechanical behavior: A review, Materials 10 (1) (2017) 50.
[32] T.T. Oliveira, A.C. Reis, Fabrication of dental implants by the additive manufacturing method: A systematic review, J. Prosthetic Dentistry 122 (3) (2019) 270–274.
[33] C. Zhang, Z. Chen, J. Liu, M. Wu, J. Yang, Y. Zhu, W.W. Lu, C. Ruan, 3D-printed pre-tapped-hole scaffolds facilitate one-step surgery of predictable alveolar bone augmentation and simultaneous dental implantation, Compos. Part B: Eng. (2021) 109461.
[34] J. Li, H. Li, L. Shi, A.S. L, C. Ucer, H. Devlin, K. Horner, N. Silikas, A mathematical model for simulating the bone remodeling process under mechanical stimulus, Dental Mater. 23 (2007) 1073–1078.
[35] M. Lisiak-Myszke, D. Marciniak, M. Bieliński, H. Sobczak, Ł. Garbacewicz, B. Drogoszewska, Application of Finite Element Analysis in Oral and Maxillofacial Surgery—A Literature Review, Materials 13 (14) (2020) 3063.
[36] A. Brune, M. Stiesch, M. Eisenburger, A. Greuling, The effect of different occlusal contact situations on peri-implant bone stress–A contact finite element analysis of indirect axial loading, Mater. Sci. Eng., C 99 (2019) 367–373.
[37] F. Guo, M. Hu, C. Wang, S. Huang, M. Lou, C. Liu, Studies on the Performance of Molar Porous Root-Analogue Implant by Finite Element Model Simulation and Verification of a Case Report, J. Oral Maxillofacial Surg. 78(11) (2020) 1965. e1-1965. e9.

[38] O. Cantó-Navés, R. Medina-Galvez, X. Marimon, M. Ferrer, Ó. Figueras-Álvarez, J. Cabratosa-Termes, A 3D finite element analysis model of single implant-supported prosthesis under dynamic impact loading for evaluation of stress in the crown, abutment and cortical bone using different rehabilitation materials, Materials 14 (13) (2021) 3519.
[39] A. Robau-Porrua, Y. Pérez-Rodríguez, L.M. Soris-Rodríguez, O. Pérez-Acosta, J.E. González, The effect of diameter, length and elastic modulus of a dental implant on stress and strain levels in peri-implant bone: a 3D finite element analysis, Bio-Med. Mater. Eng. 30 (5–6) (2020) 541–558.
[40] L. Paracchini, C. Barbieri, M. Redaelli, D. Di Croce, C. Vincenzi, R. Guarnieri, Finite Element Analysis of a New Dental Implant Design Optimized for the Desirable Stress Distribution in the Surrounding Bone Region, Prosthesis 2 (3) (2020) 225–236.
[41] K. Song, Z. Wang, J. Lan, S. Ma, Porous structure design and mechanical behavior analysis based on TPMS for customized root analogue implant, J. Mech. Behav. Biomed. Mater. 115 (2021) 104222.
[42] G. Yu, Z. Li, S. Li, Q. Zhang, Y. Hua, H. Liu, X. Zhao, D.T. Dhaidhai, W. Li, X. Wang, The select of internal architecture for porous Ti alloy scaffold: A compromise between mechanical properties and permeability, Mater. Des. 192 (2020) 108754.
[43] C.-T. Pan, W.-H. Hsu, Y.-S. Cheng, Z.-H. Wen, W.-F. Chen, A New Design of Porosity Gradient Ti-6Al-4V Encapsulated Hydroxyapatite Dual Materials Composite Scaffold for Bone Defects, Micromachines 12 (11) (2021) 1294.
[44] U. Lekholm, G. Zarb, Patient selection and preparation. In: Tissue-Integrated Prostheses: Osseointe-gration in Clinical Dentistry, Quintessence, Chicago, 1985.
[45] J. León de Ulloa, A. López Cruz, J.E. González Ruíz, Y.V. Pérez Rodríguez, R. Ríos Moreno, Diseño de andamios personalizados para la regeneración de una mandíbula con dimensiones reducidas, Revista Cubana de Investigaciones Biomédicas 36 (1) (2017) 1–8.
[46] B. Liao, R.F. Xia, W. Li, D. Lu, Z.M. Jin, 3D-Printed Ti6Al4V Scaffolds with Graded Triply Periodic Minimal Surface Structure for Bone Tissue Engineering, J. Mater. Eng. Perform. (2021) 1–12.
[47] T. Li, L. Kong, Y. Wang, K. Hu, L. Song, B. Liu, D. Li, J. Shao, Y. Ding, Selection of optimal dental implant diameter and length in type IV bone: a threedimensional finite element analysis, J. Oral Maxillofac. Surg 38 (2009) 1077–1083.
[48] E.P. Pellizzer, C.A. Lemos, D.A. Almeida, V.E. de Souza Batista, J.F.S. Júnior, F.R. Verri, Biomechanical analysis of different implant-abutments interfaces in different bone types: an in silico analysis, Mater. Sci. Eng., C 90 (2018) 645–650.
[49] J. Li, J.A. Jansen, X.F. Walboomers, J.J. van den Beucken, Mechanical aspects of dental implants and osseointegration: A narrative review, J. Mech. Behav. Biomed. Mater. 103 (2020) 103574.
[50] E. Pérez-Pevida, A. Brizuela-Velasco, D. Chávarri-Prado, A. Jiménez-Garrudo, F. Sánchez-Lasheras, E. Solaberrieta-Méndez, M. Diéguez-Pereira, F.J. Fernández-González, B. Dehesa-Ibarra, F. Monticelli, Biomechanical consequences of the elastic properties of dental implant alloys on the supporting bone: finite element analysis, Biomed. Res. Int. 2016 (2016).
[51] V. Weißmann, J. Wieding, H. Hansmann, N. Laufer, A. Wolf, R. Bader, Specific yielding of selective laser-melted Ti6Al4V open-porous scaffolds as a function of unit cell design and dimensions, Metals 6 (7) (2016) 166.
[52] A. Molinari, J. Klarin, F. Johansson, M. Benedetti, V. Fontanari, E. Magalini, V. Luchin, G. Zappini, Mechanical Properties of Porous Structures Produced by Selective Laser Melting of a Ti6Al4V Alloy Powder, J. Jpn. Soc. Powder Powder Metall. 65 (8) (2018) 481–485.
[53] L. Himmlova, A. Kácovský, S. Konvičková, Influence of implant length and diameter on stress distribution: a finite element analysis, J. Prosthetic Dentistry 91(1) (2004) 20-25.
[54] K. Moiduddin, S.H. Mian, H. Alkhalefah, U. Umer, Digital design, analysis and 3D printing of prosthesis scaffolds for mandibular reconstruction, Metals 9 (5) (2019) 569.
[55] D. Luo, Q. Rong, Q. Chen, Finite-element design and optimization of a three-dimensional tetrahedral porous titanium scaffold for the reconstruction of mandibular defects, Med. Eng. Phys. 47 (2017) 176–183.
[56] Y. Xiong, W. Wang, R. Gao, H. Zhang, L. Dong, J. Qin, B. Wang, W. Jia, X. Li, Fatigue behavior and osseointegration of porous Ti-6Al-4V scaffolds with dense core for dental application, Mater. Des. 195 (2020) 108994.
[57] S. Muñoz, S. Castillo, Y. Torres, Different models for simulation of mechanical behaviour of porous materials, J. Mech. Behav. Biomed. Mater. 80 (2018) 88–96.
[58] D. Lin, Q. Li, W. Li, M. Swain, Dental implant induced bone remodeling and associated algorithms, J. Mech. Behav. Biomed. Mater. 2 (5) (2009) 410–432.
[59] Z. Fan, H. Feng, Study on selective laser melting and heat treatment of Ti-6Al-4V alloy, Results Phys. 10 (2018) 660–664.
[60] R. Pérez, J. Gargallo, P. Altuna, M. Herrero-Climent, F. Gil, Fatigue of narrow dental implants: Influence of the hardening method, Materials 13 (6) (2020) 1429.
[61] M. Niinomi, Fatigue characteristics of metallic biomaterials, Int. J. Fatigue 29 (6) (2007) 992–1000.
[62] G. Hannink, J.C. Arts, Bioresorbability, porosity and mechanical strength of bone substitutes: what is optimal for bone regeneration?, Injury 42 (2011) S22–S25
[63] M. Quirynen, I. Naert, D. van Steenberghe, Fixture design and overload influence marginal bone loss and fixture success in the Branemark system, Clin. Oral Implant Res. 3 (1992) 104–111.
[64] T. Yu, H. Gao, T. Liu, Y. Huang, C. Wang, Effects of immediately static loading on osteointegration and osteogenesis around 3D-printed porous implant: A histological and biomechanical study, Mater. Sci. Eng., C 108 (2020) 110406.
[65] H.M. Frost, Bone's mechanostat: a 2003 update, Anatomical Record Part A 275 (2) (2003) 1081–1101.
[66] H.M. Frost, A 2003 update of bone physiology and Wolff's Law for clinicians, Angle Orthodontist 74 (1) (2004) 3–15.
[67] J.F. Valera-Jiménez, G. Burgueño-Barris, S. Gómez-González, J. López-López, E. Valmaseda-Castellón, E. Fernández-Aguado, Finite element analysis of narrow dental implants, Dent. Mater. 36 (7) (2020) 927–935.